frontiers | Frontiers in Materials

TYPE Original Research
PUBLISHED 04 December 2024
DOI 10.3389/fmats.2024.1416246

OPEN ACCESS

EDITED BY
Pawel Polaczyk,
Texas Tech University, United States

REVIEWED BY
Sandesh Pandey,
Texas Tech University, United States
Johannes Büchner,
TU Braunschweig, Germany
Jason Moore,
Federal Highway Administratin-EFLHD,
United States

*CORRESPONDENCE
Yanhui Niu,
niuyh@chd.edu.cn

RECEIVED 12 April 2024
ACCEPTED 08 October 2024
PUBLISHED 04 December 2024

CITATION
Niu Y, Wang X, Burmistrov I and Niu D (2024) Rheological properties and 3D printability of SBS/CR-modified asphalt binder with C9 petroleum resin for crack filling.
Front. Mater. 11:1416246.
doi: 10.3389/fmats.2024.1416246

Rheological properties and 3D printability of SBS/CR-modified asphalt binder with C9 petroleum resin for crack filling

Yanhui Niu[1]*, Xinyu Wang[1], Igor Burmistrov[2] and Dongyu Niu[1]

[1]School of Materials Science and Engineering, Chang'an University, Xi'an, Shaanxi, China, [2]Engineering Center, Plekhanov Russian University of Economics, Moscow, Russia

Introduction: This study investigates rheological behavior and 3D printability of SBS-, CR-, SBS/CR-modified asphalt binder with C9 petroleum resin (C9PR) for crack filling.

Methods: Thirteen types of modified asphalt binders with respective C9PR of 0 wt%, 1 wt%, 2 wt%, 3 wt% were prepared and evaluated for their microstructure, physical properties, compatibility, rheological properties, and 3D printability.

Results: The results show that SBS, CR, and C9PR influenced significantly on rheological properties and 3D printability of modified asphalt binders. Physical blending and improved storage stability of modified asphalt binders were observed with the addition of C9PR. In addition, the combination of SBS and CR showed enhanced viscoelastic behavior and temperature sensitivity compared to the base asphalt binder due to the increased swelling behavior of SBS and CR in asphalt binders by C9PR.

Discussion: Asphalt binder with 3 wt% SBS, 15 wt% CR, and 1 wt% C9PR showed improved viscosity, elasticity, compatibility, high-temperature rutting resistance, and fatigue resistance. Additionally, C9PR expanded 3D printable temperature range of modified asphalt binder, leading to its potential use as an additive in 3D printed asphalt binders.

KEYWORDS

styrene–butadiene–styrene, crumb rubber, C9 petroleum resin, rheological properties, compatibility, 3D printability, 3D-printed asphalt binder

1 Introduction

Pavement cracks easily cause surface water or other harmful substances to enter the surface layer and road base, resulting in the structural damage of the road and driving hazards (Zhang et al., 2023). In China, cracks are often treated by measures such as crack filling and crack banding (Cao et al., 2022; Li et al., 2017). However, these traditional maintenance methods have problems, such as low construction efficiency, difficulty in ensuring the safety of construction workers, and maintenance effects affected by environmental factors. In recent years, 3D printing technology has been gradually applied in the field of road engineering, especially in the crack repair project of asphalt pavements, due to its advantages of

automation, precision, and rapidity. It can effectively improve the level of engineering automation, ensure the quality of crack repair, and reduce safety risks faced by staff (Jackson et al., 2018; Ma et al., 2017).

As a new type of pavement crack-repair material, 3D-printed asphalt binder needs to have good high-temperature rheological properties and printability, and it is difficult to satisfy these requirements using base asphalt binder (Aamer et al., 2022; Gong et al., 2023). High-quality modified asphalt binders commonly used in engineering include styrene–butadiene–styrene (SBS)-modified asphalt binder and crumb rubber (CR)-modified asphalt binder. SBS is commonly used to modify asphalt binder for improving both high- and low-temperature performance, and CR is commonly used to improve viscoelastic properties. However, it is still difficult to satisfy the requirements of 3D printing technology to repair cracks using single-modifier-modified asphalt binders. The lower workability and higher production cost of SBS-modified asphalt binder limit its application. CR-modified asphalt binder is also difficult to handle due to its poor processability, and it cannot be stored for a long time due to its phase separation problems. At the same time, the swelling process of CR usually requires continuous stirring of the mixture at high temperatures, which imposes higher requirements on the preparation process (Mturi et al., 2014; Presti, 2013; Shatnawi and President, 2010). SBS/CR composite-modified asphalt binder makes up for the insufficient performance of the single-modifier-modified asphalt binder, but there is still a problem of insufficient compatibility, which makes it difficult to satisfy the printability requirements of 3D-printed asphalt binder.

In face of the limitations of traditional CR-modified asphalt binder, an alternative material called wet-process terminal blend has attracted more and more attention. This alternative material overcomes the problem of segregation by using less and finer CR and introducing high-temperature shear (Cai et al., 2014; Presti, 2013; Presti et al., 2012). Unlike the swelling mechanism of general CR, terminal blend technology primarily relies on the desulfurization or depolymerization of rubber in hot asphalt binder and the full dispersion of rubber in the blend to obtain a homogeneous and stable modified binder (Presti, 2013; Presti et al., 2012; Zhang J. et al., 2021). Researchers have found that terminal blend binder has many advantages, such as good workability, especially suitable for dense graded mixtures, and is suitable for almost all fields where traditional CR asphalt binder can be used (Cai et al., 2014; Presti, 2013; Presti et al., 2012; Shatnawi and President, 2010). However, terminal blend binder still needs to solve many problems before it is widely used in engineering. For example, the deformation and fatigue resistance of the terminal blend binder may be reduced due to reduced viscosity and elasticity loss caused by the desulfurization effect (Glover et al., 2000; Presti, 2013; Presti et al., 2012). In response to the above, SBS is often used to modify terminal blend binder to compensate for the loss of viscosity and elasticity (Presti, 2013; Shatnawi and President, 2010; Zhang W. et al., 2021). However, SBS- and terminal blend–CR composite-modified asphalt binder still has the problem of insufficient compatibility. Based on this, C9 petroleum resin (C9PR) was considered a compatibilizer (Wu et al., 2022; Zhang J. et al., 2021; Zhao and Dong, 2021).

C9PR, also known as aromatic petroleum resin, is a functional resin polymerized from an unsaturated C9 fraction, a by-product of the petrochemical industry, containing unsaturated bonds and a benzene ring structure. It is easily soluble in organic solvents and characterized by good compatibility with thermoplastic rubber, a high softening point, good aging resistance, and low price. Zhang W. et al. (2021) and Wu et al. (2022) found that petroleum resin can promote the swelling behavior of polymer in asphalt binder by reducing the particle size of the polymer modifier and finally improve the high- temperature performance of the modified asphalt binder. Cong et al., (2016) found that the high-temperature performance of SBS-modified asphalt binder with C9PR was better than that of the SBS-modified asphalt binder. Li Z. et al. (2019), Nie et al. (2019a), and Nie et al. (2019b) found that adding C9PR to the SBS/asphalt binder/oil mixture can further improve the compatibility of SBS and asphalt binder without increasing the oil content and effectively reduce the negative reaction caused by the addition of aromatic oil while increasing viscosity. However, Kim et al. (2020) found that the viscosity of composite-modified asphalt binder with C9PR was reduced. Cong et al. (2016) and Gong et al. (2022) found that when the C9PR level exceeded a certain amount, the viscosity of polymer-modified asphalt binder decreased. Most scholars have added C9PR to modified asphalt binders with a high SBS content (such as 6% and 8%) and concluded that the improvement in the performance of asphalt binder is proportional to the content of C9PR. However, according to a few researchers, C9PR has a peak effect on the performance improvement of modified asphalt binder when using SBS-modified asphalt binder purchased directly from certain companies. This means that the effect of C9PR on the performance of SBS-modified asphalt binder is not only closely related to the content of C9PR but also closely related to the content of SBS. In most studies on SBS-modified asphalt binders, researchers replaced part of SBS by adding a certain amount of CR with the aim of increasing economy and sustainability while maintaining performance. Therefore, it is necessary to study the effect of C9PR on the performance of the lower-content modifier-modified asphalt binder in the context of sustainable development.

Based on the above discussion, this study selected SBS and CR (treated by terminal blend) as the main modifiers and selected C9PR as an additive and compatibilizer to prepare modified asphalt binders. The road performance of modified asphalt binders was evaluated using microscopic tests, physical property tests, and rheological tests. The effect of C9PR on the performance of binders was investigated. After the performance tests, suitably modified asphalt binders were selected for 3D printing tests to verify whether the prepared modified asphalt binders show potential to be used as crack-filling material for 3D printing. The purpose of this study was to prepare a modified asphalt binder suitable for 3D printing to fill and repair cracks. A technical flowchart of this paper is shown in Figure 1.

2 Materials

The base asphalt binder used in this study was SK-70 road petroleum asphalt binder. SBS used in this study was T161B linear SBS produced by Xinjiang Dushanzi Petrochemical Company, and its block ratio was 30:70. In this study, 80 mesh CR was used, and C9PR used in this study was produced by Shandong Yousuo Chemical Technology Co., Ltd. Modified asphalt binders

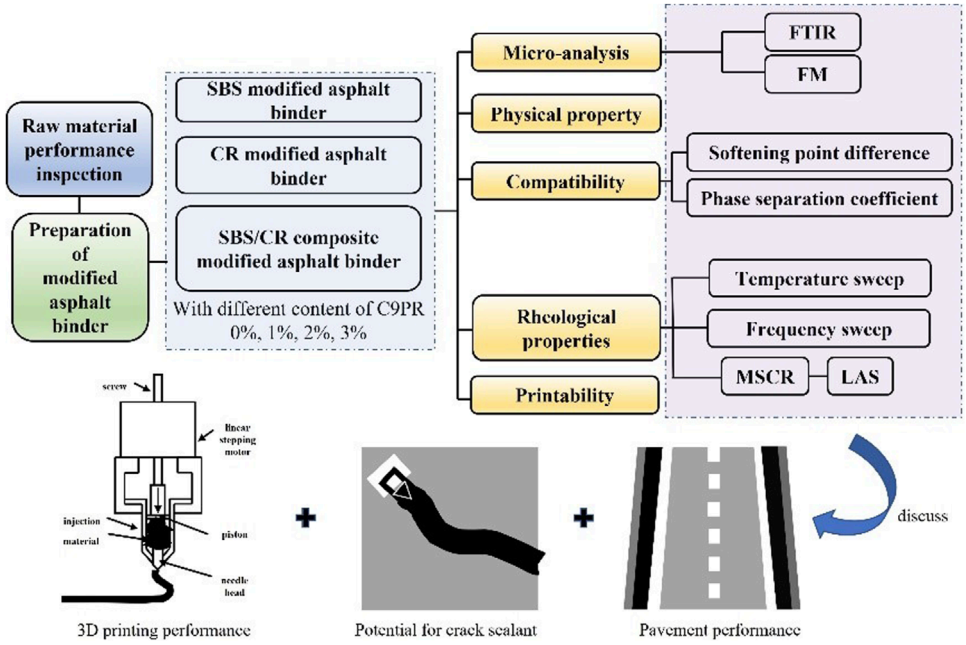

FIGURE 1
Experimental flow diagram.

were prepared with C9PR of 0 wt%, 1 wt%, 2 wt%, and 3 wt%, respectively.

(1) The base asphalt binder was heated to approximately 200°C. After adding 15 wt% CR, it was quickly heated to 220°C and sheared at a high speed of 5,000 r/min for 1 h. This step needs to be omitted for modified asphalt binders with SBS alone (Cai et al., 2014; Presti, 2013; Presti et al., 2012).
(2) The base (or modified) asphalt binder was cooled (or heated) to approximately 175°C; 3 wt% SBS and C9PR with different contents were added; and after keeping temperature dissolved for 30 min, the asphalt binder was sheared at a high speed of 5,000 r/min for 1 h.
(3) Then, a 0.15-wt% sulfur stabilizer was added to the modified asphalt binder, and the binder was sheared at a high speed of 5,000 r/min for 20 min.
(4) Finally, the asphalt binder sample was heated in an oven at 165 C for 30 min.

The abbreviated name of each modified asphalt binder sample is shown in Table 1.

TABLE 1 Detailed information about asphalt binders.

Designation	Asphalt binder
BA	Base asphalt binder
S_3	3 wt% SBS
S_3C_1	3 wt% SBS + 1 wt% C9PR
S_3C_2	3 wt% SBS + 2 wt% C9PR
S_3C_3	3 wt% SBS + 3 wt% C9PR
R_{15}	15 wt% CR
$R_{15}C_1$	15 wt% CR + 1 wt% C9PR
$R_{15}C_2$	15 wt% CR + 2 wt% C9PR
$R_{15}C_3$	15 wt% CR + 3 wt% C9PR
S_3R_{15}	3 wt% SBS + 15 wt% CR
$S_3R_{15}C_1$	3 wt% SBS + 15 wt% CR + 1 wt% C9PR
$S_3R_{15}C_2$	3 wt% SBS + 15 wt% CR + 2 wt% C9PR
$S_3R_{15}C_3$	3 wt% SBS + 15 wt% CR + 3 wt% C9PR

3 Measurement

3.1 Fourier-transform infrared spectroscopy

In this study, Fourier-transform infrared (FTIR) spectroscopy was conducted using a Bruker TENSOR II FTIR spectrometer equipped with a reflection diamond ATR accessory. Scans within wavenumbers ranging from 400 cm^{-1} to 4,000 cm^{-1} were obtained and averaged for each sample. The intensity of the FTIR spectrum can be plotted as the percentage of light transmittance or absorbance at each wavenumber. The spectrum baseline correction was performed using OMNIC software.

3.2 Fluorescence microscopy

In this study, the Imager.Z2 electric fluorescence microscope (FM) of Carl Zeiss Optics Co., Ltd., Germany, was used to excite the asphalt binder samples by using an ultraviolet light source with a short wavelength and high frequency filtered by a point-light source of high-efficiency light emittance, and the micro-morphological characteristics of each modified asphalt binder sample were observed. The dispersion effect of the modifier and its compatibility with the asphalt binder were analyzed and evaluated. The samples were observed at an ambient temperature and 200× magnification.

3.3 Physical properties

In this study, the 25-C penetration, softening point, 15-C ductility, and rotational viscosity of modified asphalt binders were tested according to the Standard Test Methods of Bitumen and Bituminous Mixture for Highway Engineering (JTG E20-2011). The elastic recovery rate and cone penetration of the modified asphalt binders were tested according to the Standard Test Method of Hot-poured Sealants for Pavement (JT/T 740-2015).

3.4 Compatibility

The phase separation of polymer-modified asphalt binders is a serious issue in the asphalt binder industry. Therefore, a hot storage test is necessary to characterize the high-temperature storage stability of modified binders during transportation and storage periods. Experimental methods and analytical approaches were combined with Chinese Standard JTG E20-2011 and European Standard EN 13399 methods. Approximately 35 g modified binder was poured into an aluminum cigar tube (32-mm diameter and 160-mm height), and then, the tube was sealed carefully using pliers. The tube was moved to an oven and kept vertically at 163°C ± 5°C for 48 h. Then, the cigar tube was taken out of the oven and cooled in a refrigerator at 5°C for 4 h. Subsequently, the frozen cigar tubes were cut into three equal sections. The samples from the top and bottom sections were utilized and evaluated for storage stability using the softening point test (experimental methods and equipment follow JTG E20-2011) (Galooyak et al., 2010; Hallmark-Haack et al., 2019; Leng et al., 2018; Qian et al., 2018; Qian et al., 2019) and segregation index (SI) [obtained from the dynamic shear rheometer (DSR) test results]. SI was defined as the following equation (Hallmark-Haack et al., 2019; Hosseinnezhad et al., 2019; Kabir et al., 2020; Li Z. et al., 2019; Xu et al., 2017; Yu et al., 2018):

$$SI = \frac{\left(\frac{G^*}{\sin\delta}\right)_{max} - \left(\frac{G^*}{\sin\delta}\right)_{avg}}{\left(\frac{G^*}{\sin\delta}\right)_{avg}},$$

where $(G^*/\sin\delta)_{max}$ is the higher value of either the top or bottom section of the cigar tube and $(G^*/\sin\delta)_{avg}$ is the average value of both sections. G^* and δ were measured using the Superpave 102 DSR. The test temperature was set to 60°C, the shear strain was set to 0.1%, and the loading frequency was 10 rad/s. The smaller the SI value, the better the compatibility between the modifiers and asphalt binders.

3.5 Temperature sweep

The temperature scanning program in the DSR was used to test the high-temperature deformation resistance of modified asphalt binders. In this test, a flat rotor with a diameter of 25 mm was selected. The flat gap was 1 mm; the test temperature was set at 30°C, 40°C, 50°C, 60°C, 70°C, and 80°C; the strain level was 0.1%; and load frequency was fixed at 10 rad/s. The phase angle and rutting factor were used to evaluate the shear deformation resistance and high-temperature performance of the modified asphalt binders.

3.6 Frequency sweep

The frequency scanning test program in the DSR was used to test the modified asphalt binder samples to obtain the rheological parameters of asphalt binder samples at different loading frequencies, loading temperatures, and shear stress levels. In the frequency scanning test program, a 25-mm parallel plate was selected for the test rotor, and the plate gap was 1 mm. The load frequency range was 0.1 Hz ~ 100 Hz; the temperature range was 30°C, 40°C, 50°C, 60°C, 70°C, and 80°C; and the shear strain value was controlled to be 0.1%. According to test results, the Williams–Landel–Ferry (WLF) function was used to fit displacement factors of all samples with 35°C as a reference temperature, and the generalized logistic sigmoidal model was used to fit the complex shear modulus and phase angle based on the time–temperature superposition principle (Rowe and Sharrock, 2009; Yusoff et al., 2011).

3.7 Multiple stress creep–recovery

The multiple stress creep–recovery (MSCR) test is used to characterize modified asphalt binders and has good correlations with asphalt mixture rutting. The MSCR test was performed on a DSR to test elastic recovery behavior and stress-dependent behavior at 64°C under a creep stress of 0.1 kPa and 3.2 kPa, following AASHTO MP 19. Before the test, all asphalt binders were subjected to the short-term aging treatment (Rolling Thin-Film Oven Test, RTFOT). Two stress levels of 0.1 kPa and 3.2 kPa were used, of which 20 creep (1 s)–recovery (9 s) cycles were performed at the stress level of 0.1 kPa, and 10 cycles were performed at the stress level of 3.2 kPa for a total of 300 s. The stress-dependent behavior and unrecoverable behavior of binders were characterized by the creep characteristics of samples during the 100 s–300-s loading cycle.

3.8 Linear amplitude sweep

According to AASHTO TP101, the fatigue performance of the modified asphalt binders was studied by the linear amplitude scanning (LAS) test. LAS test samples were all asphalt binder samples after 20 h of pressure aging vessel (PAV). DSR equipment was used in this test, and the temperature was set to 25°C. The LAS test program mainly includes two stages. In the first stage,

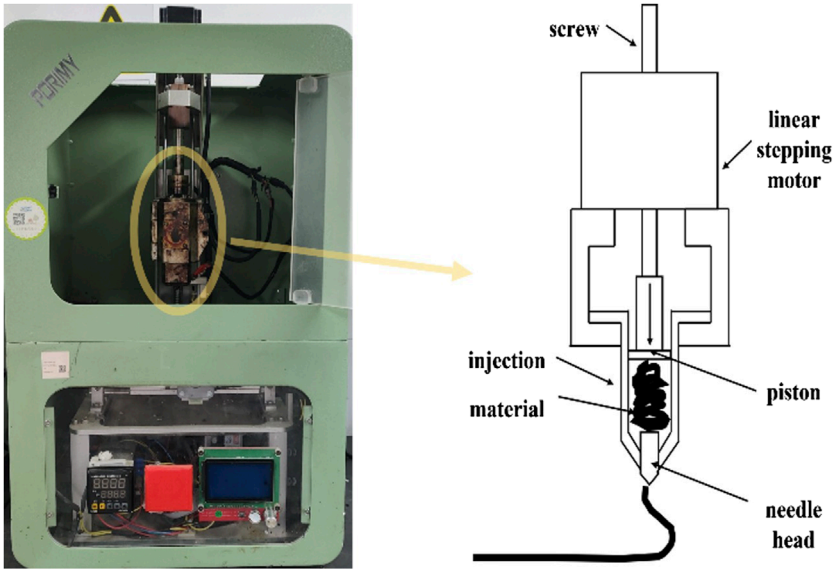

FIGURE 2
3D printer: internal structure and key equipment.

a frequency scan with a constant shear strain amplitude of 0.1% was applied to the samples, and the loading frequency range was 0.2 Hz~30 Hz to obtain the undamaged rheological properties of asphalt binder samples in the LVE range. In the second stage, amplitude scanning was performed on the samples to obtain the damage characteristics of asphalt binder samples, in which the oscillatory shear strain increased linearly from 0% to 30% within 5 min at a loading frequency of 10 Hz. After the test, the predicted fatigue life of each modified asphalt binder was calculated by VECD theory (Park et al., 1996).

3.9 3D printing

The 3D printer used in this study is a plunger extruder and is shown in Figure 2. The printer is designed as a three-axis system, in which the needle head is moved by a single-stepper motor to print to a flat plate. The printer is composed of an extrusion plunger, a stepper motor driving the screw, a heating barrel, and a printing needle head. The maximum print size is 100 mm × 100 mm × 50 mm.

4 Results and discussion

4.1 FTIR analysis

The FTIR spectroscopy results and functional groups corresponding to the characteristic absorption peaks of C9PR, BA, and each modified asphalt binder are shown in Figure 3 and Table 2, respectively. Figure 3A shows that the absorption peak of C9PR at 3,445 cm^{-1} is the stretching vibration absorption peak of -OH. The absorption peak at 3,000~3,100 cm^{-1} is the stretching vibration absorption peak of olefin C-H and aromatic compound C-H. The absorption peak at 2,900~3,000 cm^{-1} is the antisymmetric stretching vibration absorption peak of -CH2-. The absorption peak at 1,500~1,700 cm^{-1} is the vibration absorption peak of the olefin double bond and benzene ring skeleton. The absorption peak at 1,479 cm^{-1} is generated by the vibration of the C-S bond, indicating that C9PR contains other impurity atoms in addition to C and H. The absorption peak at 1,032 cm^{-1} is the sulfoxide absorption peak. The absorption peak at 748 cm^{-1} is the absorption peak of the substituent on the benzene ring. The absorption peak at 699 cm^{-1} is the C-H vibration absorption peak on the benzene ring of the polystyrene segment.

Figures 3B–D show that the infrared spectrum of the SBS-modified asphalt binder has obvious absorption peaks at 966 cm^{-1} and 699 cm^{-1}, which is the result of C-H vibration on the carbon–carbon double bond of the polybutadiene segment and benzene ring of the polystyrene segment in the SBS component, respectively. Compared with the single-modifier-modified asphalt binder, the SBS/CR composite-modified asphalt binder has no new characteristic peak, but the absorption peak intensity at 1,600, 1,455, 1,375, 966, and 699 cm^{-1} is weakened, which indicates that in the process of SBS and CR composite modification, chemical reactions mainly occur on the conjugated double bond on the benzene ring, i.e., $-CH_3$, $-CH_2-$, -C=C-, and C-H on the benzene ring, among which the absorption peak intensity at 966 cm^{-1} (-C=C-) changes most obviously. This is because -C=C- is unstable, easily opens during heating and shearing, and has strong activity after opening, thus undergoing a branching reaction with CR.

With the increase in the C9PR content, no new characteristic peaks appeared in each modified asphalt binder, indicating that the modification effect of C9PR on each modified asphalt binder was physical and no chemical change occurred. With the increase in

10.3389/fmats.2024.1416246

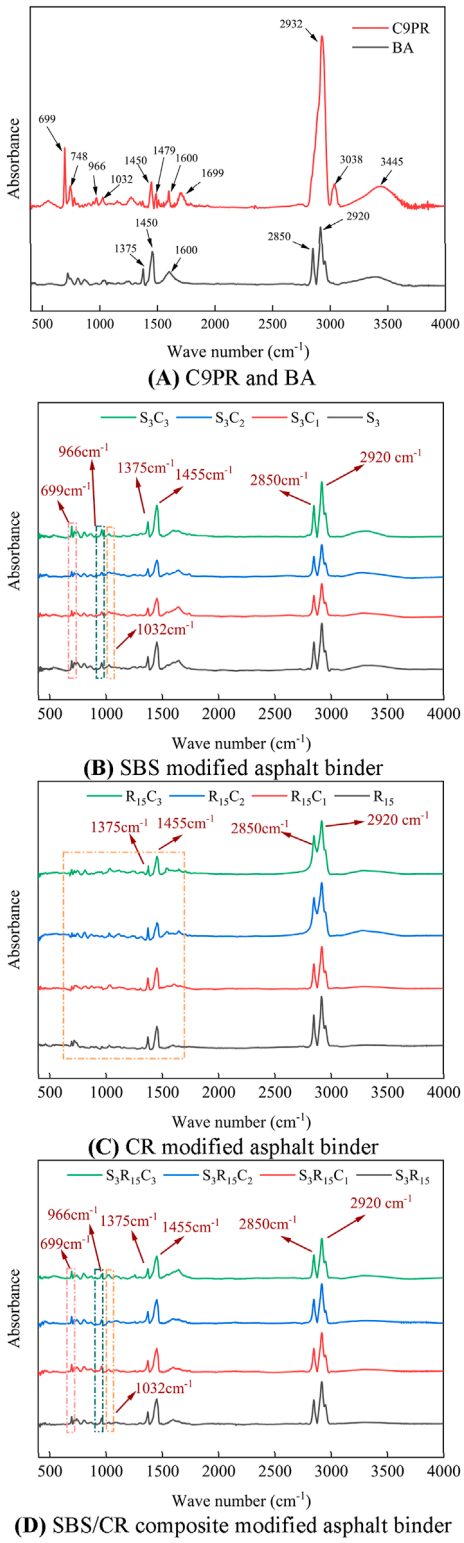

FIGURE 3
FTIR spectra of C9PR, BA, and modified asphalt binders. **(A)** C9PR and BA. **(B)** SBS-modified asphalt binder. **(C)** CR-modified asphalt binder. **(D)** SBS/CR composite-modified asphalt binder.

the C9PR content, the peak area at 900~650 cm^{-1} of each modified asphalt binder increased slightly, indicating that C9PR introduced aromatics into the modified asphalt binder system.

TABLE 2 Location of absorption peaks and corresponding functional groups in the infrared spectra of modified bituminous binders (Hou et al., 2018).

Peak position/cm^{-1}	Functional groups and vibrational types
3,400	Stretching vibration of -OH
2,920	Antisymmetric stretching vibration of -CH_2-
2,850	Symmetric stretching vibration of -CH_2-
1,600	Conjugated double bond (benzene ring backbone vibration)
1,455	-C-H stretching vibration in CH_3 (variable angle vibration)
1,375	C-H surface stretching vibration (bending vibration) in -CH_2-
1,032	Sulfinyl group -S=O
966	Polybutadiene segment -C=C-
813	C-H out-of-plane bending vibration on the benzene ring
699	C-H vibration on the benzene ring of the polystyrene segment

4.2 FM analysis

FM images of each modified asphalt binder magnified 200 times are shown in Figure 4. Comparing images of each sample showed that the different fluorescence characteristics of BA and polymer modifiers lead to obvious color differences between two phases in a miscible system. The brighter fluorescence points are various modifier particles, while C9PR and BA are similar in color under the fluorescence microscope. Figures 4A–D show that SBS modifier particles are large, and the dispersion in the asphalt binder is not uniform. However, with the increase in C9PR incorporation, the size of SBS particles gradually decreases, and the distribution gradually becomes uniform.

From Figures 4E–L, it can be found that CR-modified asphalt binder and SBS/CR composite-modified asphalt binder showed similar rules. This may be because C9PR, which is rich in aromatics, can promote the swelling of SBS and CR in the asphalt binder, thus promoting the swelling of modifier particles in the preparation process of modified asphalt binders. Particles are sheared into smaller particles at high speed, which ultimately increases the dispersion and compatibility of each modifier in the asphalt binder. Therefore, C9PR shows potential to be an additive used to increase the 3D printing performance of modified asphalt binders.

4.3 Physical property analysis

Table 3 shows that with the increase in C9PR content, the penetration and cone penetration of each modified asphalt binder decrease. The softening point of each modified asphalt binder

10.3389/fmats.2024.1416246

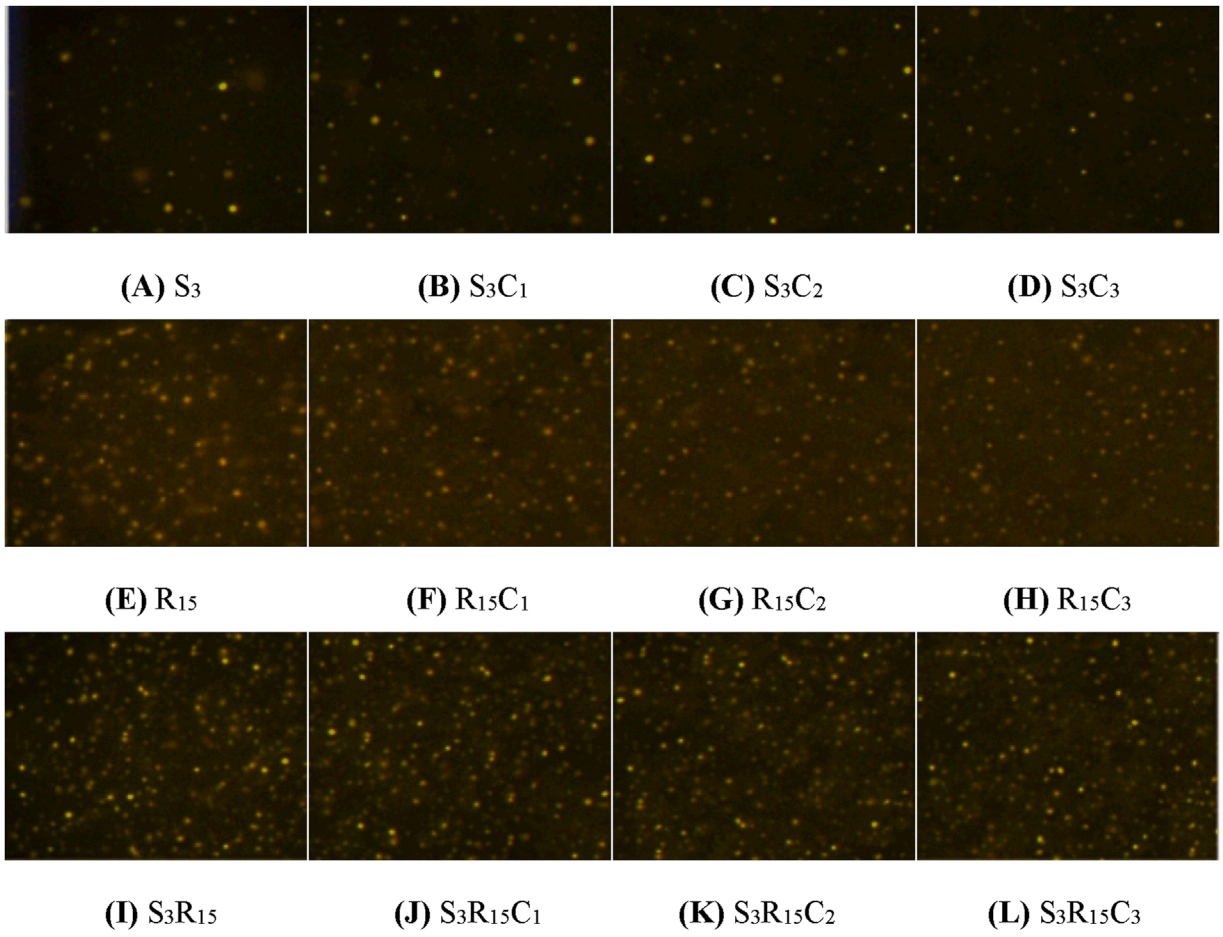

FIGURE 4
FM images of each modified asphalt binder. **(A)** S_3. **(B)** S_3C_1. **(C)** S_3C_2. **(D)** S_3C_3. **(E)** R_{15}. **(F)** $R_{15}C_1$. **(G)** $R_{15}C_2$. **(H)** $R_{15}C_3$. **(I)** S_3R_{15}. **(J)** $S_3R_{15}C_1$. **(K)** $S_3R_{15}C_2$. **(L)** $S_3R_{15}C_3$.

increases with the increase in C9PR content, but the increasing trend gradually weakens. This may be because C9PR is rich in aromatic components, and the addition of a small amount can improve the dispersion of polymer copolymers and the uniform dispersion of modifiers. However, when the C9PR content exceeds a certain level, the enhancement effect of the polymer copolymer on modified asphalt binders is less than the compatibility effect of the aromatic component. In this case, the improvement of C9PR on the high-temperature stability of the modified asphalt binder is limited.

Rotational viscosity at 135°C of the single SBS or CR-modified asphalt binder is much smaller than that of the SBS/CR composite-modified asphalt binder, indicating that the performance of the composite-modified asphalt binder is better. The increase in the rotational viscosity of asphalt binders caused by the addition of 1 wt% C9PR may be due to the compatibilization effect of C9PR on SBS- and CR-modified asphalt binders, which promotes the performance of the modified asphalt binder. Viscosity reduction caused by C9PR with more than 1% content may be due to the excessive compatibilization of aromatics, which weakens the crosslinking effect between macromolecules, resulting in a decrease in viscosity.

With the increase in C9PR content, the ductility and elastic recovery rate of modified asphalt binders decreased slightly, and the decrease rate increased. This may be because C9PR has a rigid side-chain benzene ring. With the increase in C9PR content, modified asphalt binders show greater brittleness at low temperature, and elastic properties and low-temperature ductility are also affected.

According to JT/T 740–2015, the requirements of a high-temperature sealant are as follows: softening point ≥90°C, cone penetration ≤70 (0.1 mm), and elastic recovery 30%~70%. Combined with specification, it can be found that single-modifier-modified asphalt binders do not meet the technical requirements of various sealants in the specification, while composite-modified asphalt binders with any content of C9PR can meet the specification requirements of a high-temperature sealant.

4.4 Compatibility analysis

SBS and CR are incompatible with asphalt binder thermodynamics, and segregation will occur during storage, which will affect the road performance of the modified asphalt binder and printability as a 3D-printed asphalt binder. Therefore, based on the

10.3389/fmats.2024.1416246

TABLE 3 Physical properties of modified asphalt binders.

Asphalt binder sample	Softening point, °C	Penetration at 25°C, 0.1 mm	Ductility at 15°C, cm	Rotational viscosity at 135°C, Pa·s	Elastic recovery rate, %	Cone penetration, 0.1 mm
S_3	76.0	68.0	51.0	0.99	48.4	69.7
S_3C_1	78.0	67.0	50.0	1.36	48.0	68.1
S_3C_2	79.3	66.1	48.0	1.18	47.0	67.6
S_3C_3	79.2	65.4	45.0	0.86	45.5	67.0
R_{15}	71.0	69.0	57.0	0.91	43.6	70.1
$R_{15}C_1$	74.0	68.0	56.0	1.21	43.3	69.0
$R_{15}C_2$	76.7	66.8	53.0	1.01	42.9	68.3
$R_{15}C_3$	76.8	66.2	47.0	0.78	41.7	67.7
S_3R_{15}	88.0	46.0	34.2	3.51	47.4	50.4
$S_3R_{15}C_1$	90.1	43.0	33.2	4.09	47.0	49.0
$S_3R_{15}C_2$	90.6	42.0	31.0	3.81	46.2	48.3
$S_3R_{15}C_3$	90.6	41.0	27.1	3.08	45.3	47.2

segregation test, the effect of C9PR on the compatibility of SBS-, CR-, and composite-modified asphalt binders was evaluated by the softening point difference method and phase separation coefficient method, respectively.

The softening point difference of each modified asphalt binder is shown in Figure 5A. The results show that the softening point difference of the single SBS-modified asphalt binder and SBS/CR composite-modified asphalt binder does not satisfy the requirements of segregation softening point difference less than 2.5°C in the specification without adding C9PR. With the increase in C9PR content, the softening point difference of each asphalt binder sample showed a decreasing trend, indicating that C9PR played a positive role in the compatibility of modified asphalt binders. The compatibility effect of C9PR on the modifier and asphalt binders decreases with increasing content, which may indicate that for 3 wt% SBS and 15 wt% CR, the compatibility effect of 2 wt% C9PR is not much different from that of 3 wt% C9PR, and the compatibility effect of C9PR gradually approaches saturation.

However, some scholars believe that the softening point difference test is simple to operate and has poor detection sensitivity (Yu et al., 2018). When evaluating the compatibility of the polymer modifier and petroleum asphalt binders, the phase change in the heat storage process of the two-phase system cannot be detected. Polymer-modified asphalt binder is a viscoelastic material. The dynamic mechanical method based on rheology is very suitable to detect differences between the petroleum asphalt binder and polymer modifier. Therefore, some researchers have proposed a phase separation coefficient based on rheological test methods to evaluate the compatibility of the polymer modifier and petroleum asphalt binder (Hallmark-Haack et al., 2019; Hosseinnezhad et al., 2019; Kabir et al., 2020; Li J. et al., 2019; Xu et al., 2017; Yu et al., 2018). The degree of phase separation of the polymer modified asphalt binder calculated quantitatively by the phase separation coefficient (Equation 1) is shown in Figure 5B. With the addition of C9PR, the SI of each modified asphalt binder sample showed a decreasing trend, which indicated that the addition of C9PR was favorable to the compatibility of SBS and CR in the asphalt binder, thus improving the high-temperature storage stability of modified asphalt binders. It is worth noting that when the C9PR content increased from 0% to 3%, the SI value of S_3C_1 decreased by 7.95% compared with S_3, the SI value of S_3C_2 decreased by 5.61% compared with S_3C_1, and the SI value of S_3C_3 decreased by 2.73% compared with S_3C_2, and the CR-modified asphalt binders and SBS/CR composite-modified asphalt binders also showed a similar pattern. The trend of the SI graph is similar to that of the softening point difference graph. This proves the conclusion of the softening point difference test, i.e., C9PR promotes the compatibility of SBS, CR, and BA, and the compatibilization effect is closely related to the content of the modifier and its own content.

4.5 Temperature sweep analysis

4.5.1 Phase angle analysis

In Superpave specification, the phase angle is defined as the time lag between strain and stress under traffic loads, which is highly dependent on temperature and loading frequency. It can be used as an indicator of the viscosity and elasticity of binders. When the phase angle is close to 90°, the asphalt binder tends to exhibit the behavior of a viscous liquid, and there is no obvious elastic effect.

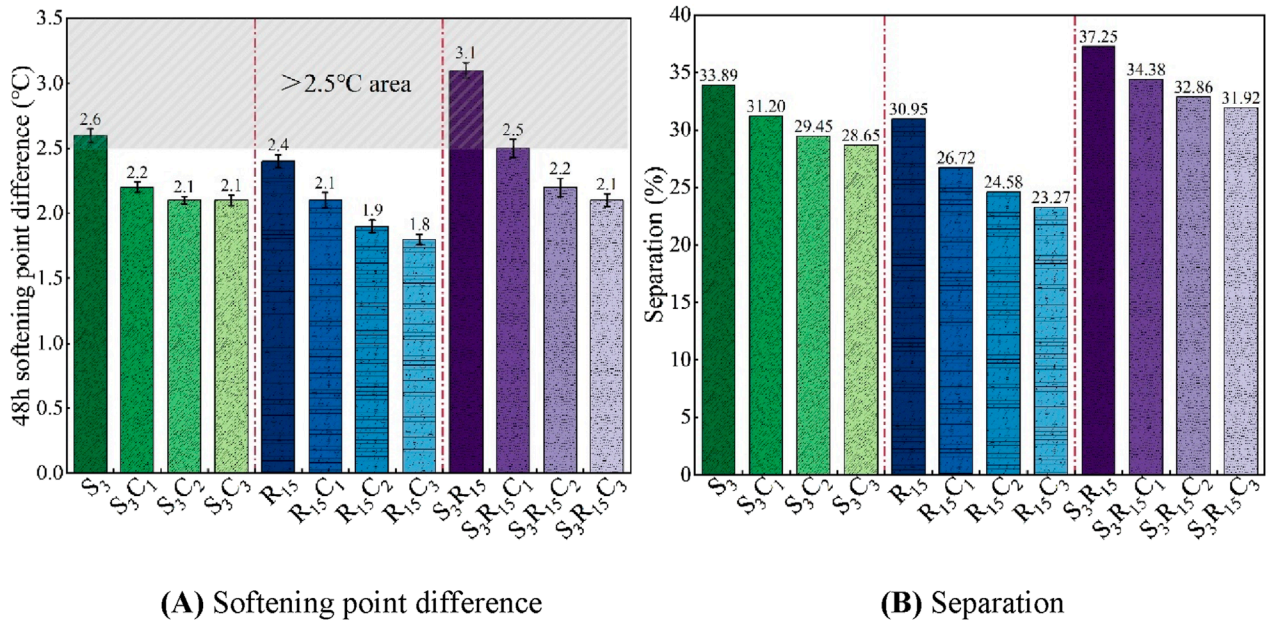

FIGURE 5
Compatibility analysis of each modified asphalt binder sample. **(A)** Softening point difference **(B)** Separation.

The relationship curve of the phase angle of each asphalt binder sample with temperature change is shown in Figure 6A. It can be seen that the trend of the phase angle of SBS-modified asphalt binders and CR-modified asphalt binders with temperature change is similar to that of BA, and both show a gradual upward trend with the increase in temperature. However, when the temperature reaches 60°C, the phase angles of S_3R_{15}, $S_3R_{15}C_1$, $S_3R_{15}C_2$, and $S_3R_{15}C_3$ peaks show an abnormal downward trend. This may be because under high-temperature conditions, the network-reinforced structure formed by the polymer dominates the rheological response of the binder and increases the friction between asphalt binder molecules. This resists the viscous flow of asphalt binders. In addition, when the content of C9PR is 1%, modified asphalt binders show a lower phase angle at different temperatures, but when the content of C9PR exceeds 1%, the phase angle increases slowly, indicating that the addition of excessive C9PR reduces the viscosity and elastic properties of modified asphalt binders.

4.5.2 Rutting factor analysis

To characterize the anti-rutting performance of the prepared asphalt binder samples, the trend curve of each asphalt binder rutting factor ($G^*/\sin\delta$) with temperature was plotted, as shown in Figure 6B. Figure 6B shows that the rutting factor decreases with the increase in temperature. In the case of high temperature, asphalt binders exhibit almost pure viscous liquid behavior, poor deformation resistance, and inability to better resist external pressure, thus becoming more prone to deformation. Under the condition of the same temperature, the type and content of the modifier have an obvious influence on the rutting factor. The experimental results showed that the order of high-temperature rutting resistance of each modified asphalt binder sample is as follows: $S_3R_{15}C_1$ > $S_3R_{15}C_2$ > S_3R_{15} > $S_3R_{15}C_3$ > S_3C_1 > S_3C_2 > S_3 > $R_{15}C_1$ > S_3C_3 > $R_{15}C_2$ > R_{15} > $R_{15}C_3$ > BA. This shows that for 3 wt% SBS and 15 wt% CR, C9PR has a critical blending value between 0% and 2%. When the content of C9PR reaches this critical value, the high-temperature anti-rutting performance of the composite-modified asphalt binder can be maximum. Once the content of C9PR exceeds this critical value, the high-temperature anti-rutting performance of the composite-modified asphalt binder will be weakened. This is consistent with the results of previous high-temperature PG classification.

4.6 Frequency sweep analysis

A temperature of 35°C was selected as the reference for drawing the master curve. Master curves of the complex shear modulus and phase angle corresponding to each modified asphalt binder sample are shown in Figure 7. Figure 7A shows that the increase in reduction frequency leads to the increase in complex shear modulus. In a low-frequency domain, the difference in the complex shear modulus of each sample is obvious. It can be found that BA has the smallest shear resistance in the same temperature and frequency range. The addition of SBS and CR will cause the master curve of the complex modulus to move up, which means that the addition of SBS or CR can improve the shear resistance of the modified asphalt binder. When the content of C9PR in each modified asphalt binder gradually increases from 0% to 3%, the master curve shows a trend of moving up first and then decreasing, which indicates that the excessive addition of C9PR has a negative impact on the deformation resistance of composite asphalt binders.

Figure 7B shows that the phase angle of each modified asphalt binder sample shows an approximately linear downward trend with the increase in the reduction frequency. In all samples, the phase

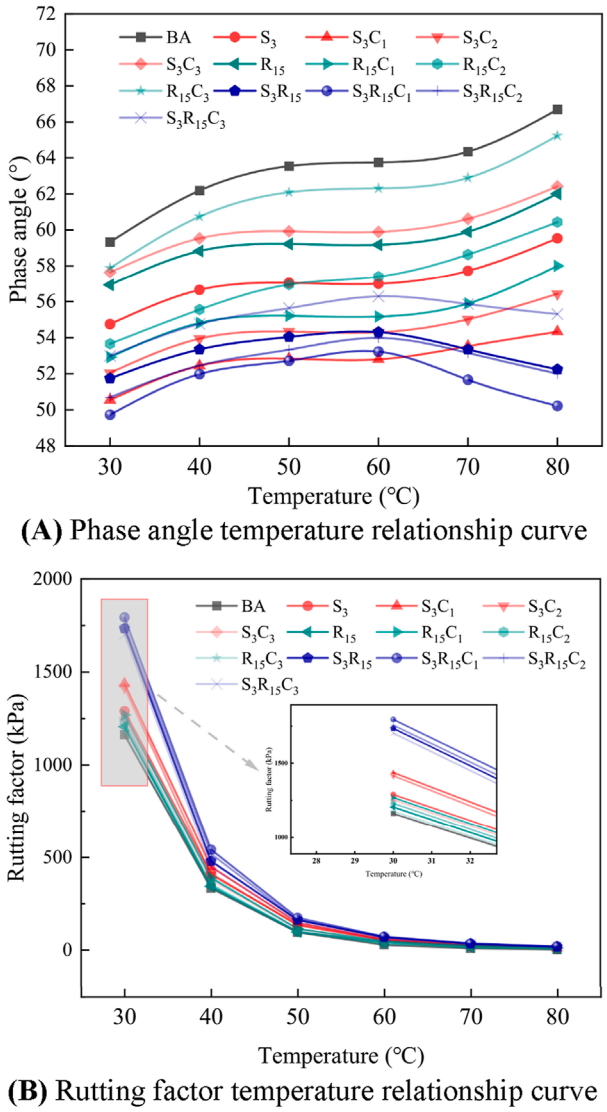

FIGURE 6
Temperature sweep analysis of each modified asphalt binder sample. **(A)** Phase angle–temperature relationship curve. **(B)** Rutting factor–temperature relationship curve.

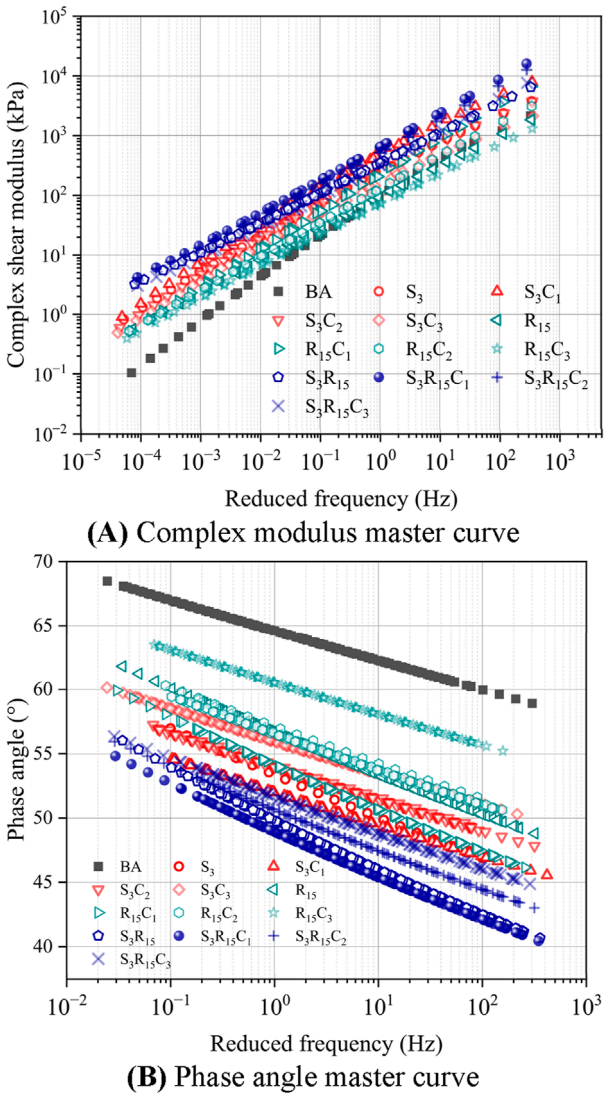

FIGURE 7
Frequency sweep analysis of each modified asphalt binder sample at 35°C. **(A)** Complex modulus master curve. **(B)** Phase angle master curve.

angle of BA is the largest, and the phase angle of $S_3R_{15}C_1$ is the smallest. The addition of SBS and CR will lead to a downward shift in the phase angle curve, indicating that both polymers can improve the shear resistance and elastic properties of the modified asphalt binder, and it is difficult to show the shear lag effect. When the content of C9PR exceeds 1%, the curve will move up again, which is consistent with the change rule of the abovementioned complex modulus master curve.

4.7 MSCR analysis

At stress levels of 0.1 kPa and 3.2 kPa, the average recovery rate and unrecoverable creep compliance of asphalt binders for 10 creep recovery cycles are expressed as R (0.1), R (3.2), J_{nr} (0.1), and J_{nr} (3.2), respectively. R represents the percentage of recoverable strain to total strain, and J_{nr} indicates the unrecoverable residual deformation. The rutting resistance of an asphalt binder with a larger R and smaller J_{nr} is stronger.

At a temperature of 64°C, R and J_{nr} of each modified asphalt binder are shown in Figure 8. Figure 8A shows that BA has the smallest R value, while the R value of the SBS/CR composite-modified asphalt binder is higher, which indicates that the SBS and CR composite can effectively improve the creep recovery ability of the asphalt binder. The test result of non-recoverable creep compliance of each sample is opposite to that of the creep recovery rate, as shown in Figure 8B. The experimental results show that the SBS/CR composite-modified asphalt binder has a smaller J_{nr} value as a whole, while BA shows a higher J_{nr} value. This shows that the presence of the SBS/CR composite modifier can inhibit the generation of irreversible deformation of the asphalt binder.

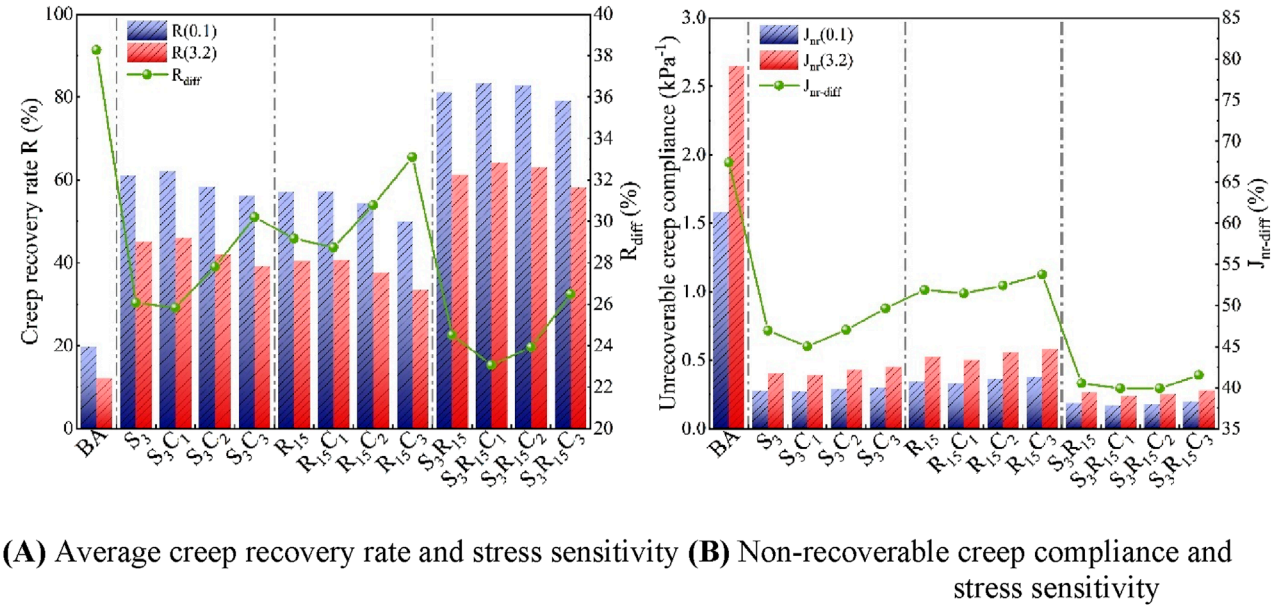

FIGURE 8
MSCR test results. **(A)** Average creep recovery rate and stress sensitivity. **(B)** Non-recoverable creep compliance and stress sensitivity.

Compared with SBS, CR single modifier, and even BA, composite modifier-modified asphalt binders show more excellent anti-rutting performance.

The effect of C9PR on the high-temperature viscoelastic properties of the modified asphalt binder obtained by the MSCR test is consistent with the high-temperature rheological test results of the unaged asphalt binder. The test results show that the increase in the C9PR content at each stress level first increases and then decreases R of each modified asphalt binder sample and first decreases and then increases J_{nr}. This shows that based on the modified asphalt binder with 3 wt% SBS and 15 wt% CR, C9PR has an optimal content in the range of 0%~2%. When the content of C9PR is optimal, C9PR plays a dominant role in compatibilization between the modifier and asphalt binder. At this time, the role of C9PR in the modified asphalt binder system is equivalent to enhancing the high-temperature elasticity of the modified asphalt binder, which is reflected in the increase in the R value and the decrease in the J_{nr} value. When C9PR exceeds its optimum content, the material properties of C9PR itself lead to a brittleness enhancement effect of the modified asphalt binder higher than the elasticity enhancement effect, which eventually leads to the decrease in the creep recovery ability and the increase in non-recoverable complex creep compliance.

To further characterize the sensitivity of each asphalt binder sample to load size, the stress sensitivity (R_{diff} and $J_{nr\text{-}diff}$) of non-recoverable creep compliance and the creep recovery rate of different binders were calculated, and the calculation results are shown in Figure 8. It can be found that $S_3R_{15}C_1$ presents the smallest R_{diff} and $J_{nr\text{-}diff}$ values, while BA has the largest R_{diff} and $J_{nr\text{-}diff}$ values, which indicates that the contents of SBS, CR, and C9PR can make the nonlinear viscoelasticity of the asphalt binder more significant. $S_3R_{15}C_1$ has a more prominent low stress sensitivity, indicating that the addition of an appropriate amount of C9PR content can make the polymer-modified asphalt binder have a more stable structure under the action of shear load.

4.8 LAS analysis

The predicted fatigue life of each asphalt binder sample calculated at two strain levels is shown in Figure 9. Under the condition of 2.5% strain, the predicted fatigue life of the single SBS-modified asphalt binder is higher than that of the single CR-modified asphalt binder, which indicates that the effect of a low content of CR on the fatigue resistance of asphalt binder is weaker than that of SBS. The fatigue life of S_3R_{15} is 5.22 times and 6.21 times higher than that of S_3 and R_{15}, respectively, which indicates that the compound content of the modifier has a great effect on the fatigue resistance of the asphalt binder. Under the condition of 5% strain, the fatigue life of each binder sample is greatly reduced, and the relationship between the fatigue lives of each asphalt binder is highly consistent with the 2.5% strain level. In general, the addition of the SBS/CR composite modifier is beneficial to improve the fatigue resistance of the asphalt binder, and this improvement effect is also prominent at a low strain level and high strain level.

The LAS test showed that the effect of C9PR on the predicted fatigue life of each modified asphalt binder was related to the dosage. Under the condition of 2.5% strain, N_f of SBS-modified asphalt binders, CR-modified asphalt binders, and SBS/CR composite-modified asphalt binders with 1 wt% C9PR increased by 3.45%, 2.10%, and 6.53%, respectively, compared with those without C9PR. When the content of C9PR is 3%, S_3C_3, $R_{15}C_3$, and $S_3R_{15}C_3$ are 5.90%, 10.01%, and 3.10% lower than S_3, R_{15}, and S_3R_{15}, respectively. The fatigue life of each modified asphalt binder increases first and then decreases with the increase in C9PR content, which is

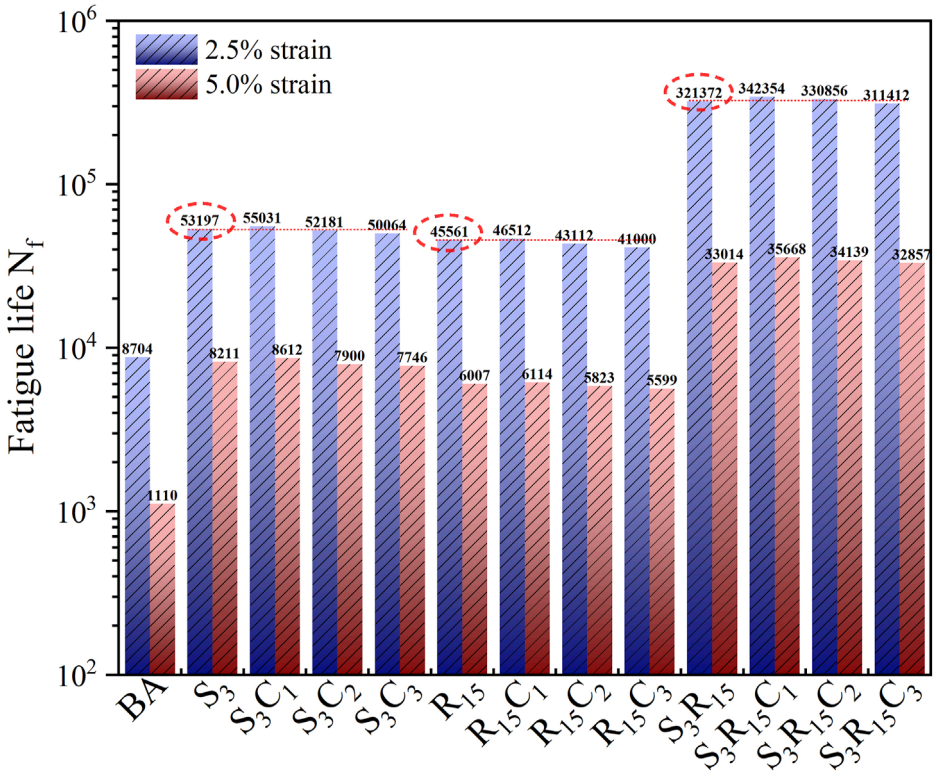

FIGURE 9
LAS test results.

consistent with the influence of C9PR on the high-temperature performance of the modified asphalt binder.

It is worth noting that when the strain condition is 2.5% and the content of C9PR is 2%, N_f of S_3C_2 and $R_{15}C_2$ is 1.91% and 5.38% lower than that of S_3 and R_{15}, respectively, indicating that the effect of 2 wt% C9PR on the fatigue life of asphalt binder exceeded the effect of 3 wt% SBS or 15 wt% single-modifier CR on the performance of the asphalt binder. N_f of $S_3R_{15}C_2$ increased by 2.95% compared with S_3R_{15} and still maintained a slight enhancement effect, which indicated that the improvement effect of C9PR on the modified asphalt binder was related to the content and type of other modifiers.

Under the condition of 5% strain, the fatigue life of each binder sample is greatly reduced, and the relationship between the fatigue lives of each modified asphalt binder is highly consistent with the 2.5% strain level. In general, the addition of SBS, CR, and an appropriate amount of C9PR content is beneficial to improve the fatigue resistance of the asphalt binder, and this improvement effect is also prominent at a low strain level and high strain level.

4.9 Analysis of the 3D printing performance of composite-modified asphalt binders

The plunger extruder used in this study softens asphalt binders by simultaneously heating the plunger sleeve and nozzle, and the softened asphalt binders are extruded through the nozzle by the motor-driven plunger. Before formal printing, the plunger is set to push slowly until the filament is extruded at the nozzle. After removing the excess material wire at the nozzle, the relevant model parameters are entered in Simplify3D slicing software (Wu, 2023; Xue, 2023; Yang, 2023).

Previous laboratory research found that when the printing temperature suitable for a certain asphalt binder was not explored, the asphalt binder could not be successfully extruded no matter how the extrusion rate of the plunger and printing speed of the equipment were changed. Once the appropriate printing temperature was obtained through the test, changing the extrusion rate of the plunger and printing speed of equipment had little effect on asphalt binder formation. This shows that the influence of temperature on the 3D-printed asphalt binder is higher than the extrusion rate and printing speed. Therefore, in this study, a 0.8-mm diameter printhead was used to adjust the printing temperature and printing speed to conduct a trial printing study of the 3D printing of composite-modified bitumen with different C9PR doping levels to explore the appropriate printing temperature, as well as to evaluate the 3D printing moldability of composite-modified bitumen. Because only the composite-modified bitumen binder meets the requirements of the sealant specification, this vignette only 3D prints the composite-modified asphalt binder for the test.

4.9.1 Printing temperature

A relatively simple line segment model printing test was carried out on the composite-modified asphalt binder with different C9PR contents. The segment model and printed results are shown in

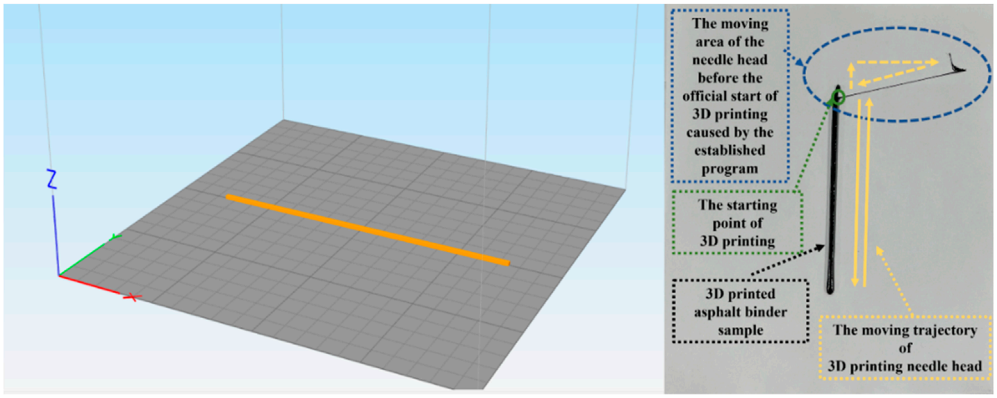

(A) Segment model for 3D printing

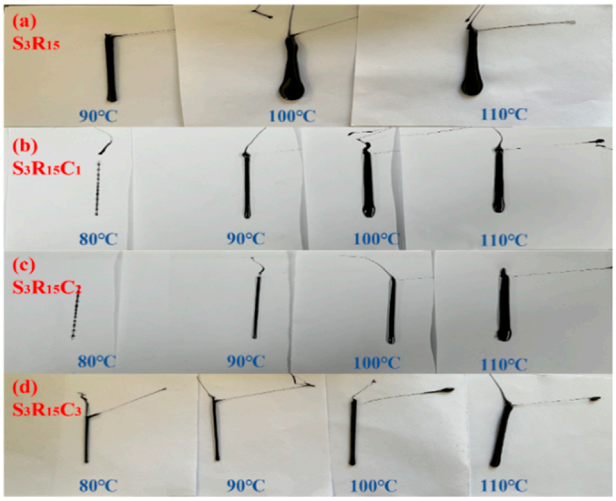

(B) Segment model printing results

FIGURE 10
Segment model and printing results of each modified asphalt binder under different temperature conditions. **(A)** Segment model for 3D printing. **(B)** Segment model printing results.

Figures 10A, B. Figure 10B shows that S_3R_{15} without C9PR failed to be successfully extruded at 80°C. At the same time, $S_3R_{15}C_1$ and $S_3R_{15}C_2$ were printed out of incoherent line segments at 80°C, which was because the asphalt binder was difficult to be extruded from the nozzle at this temperature. $S_3R_{15}C_3$ can be printed most smoothly at 80°C, which may indicate that C9PR can broaden the lower limit of temperature for the 3D-printed modified asphalt binder.

Furthermore, when the temperature increased to 90°C, segments printed by each modified asphalt binder are roughly in line with the designed model, and the thickness of line segments is relatively uniform. When temperature increases to 100°C and above, the S_3R_{15} sample segment produces obvious thickening and unevenness, while the modified asphalt binder mixed with C9PR is less affected by temperature, which indicates that C9PR has a favorable effect on the printability of the 3D-printed asphalt binder.

4.9.2 Printing speed

Print speed and the 3D printing process are a matching process; if too fast or too slow, the model cannot be printed successfully. For asphalt binder material, under a constant extrusion rate, if the nozzle moves too fast, asphalt binder material near the nozzle that has not finished adhering to the bottom will be pulled by the nozzle movement, which will affect the degree of precision of the printed object size; if the nozzle moves too slowly, it may produce a material accumulation phenomenon, which easily builds up and blocks the nozzle. According to the experimental results in the previous subsection, we consider the shape stability of the asphalt binder material extrusion; fix the printing temperature at 90°C; and select printing speeds of 2 mm/s, 4 mm/s, and 6 mm/s, respectively, to study the influence of the printing speed, i.e., the nozzle movement speed, on the 3D printability of the composite-modified asphalt binders. At the same time, we consider the existence of a certain depth and shape of the cracks in the actual application process and

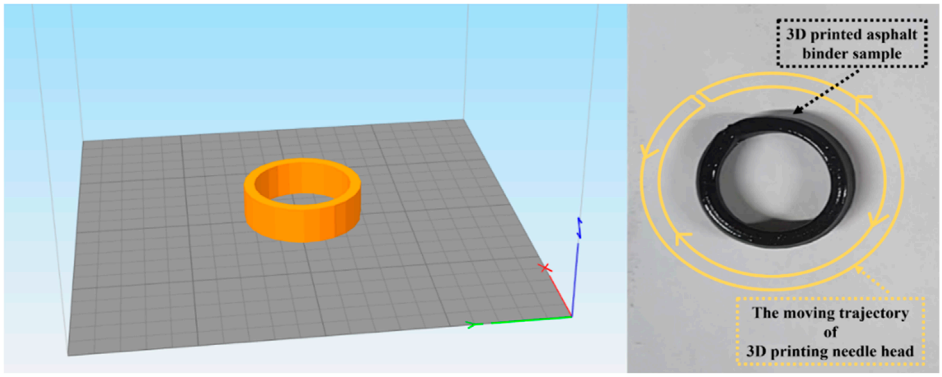

(A) Ring model for 3D printing

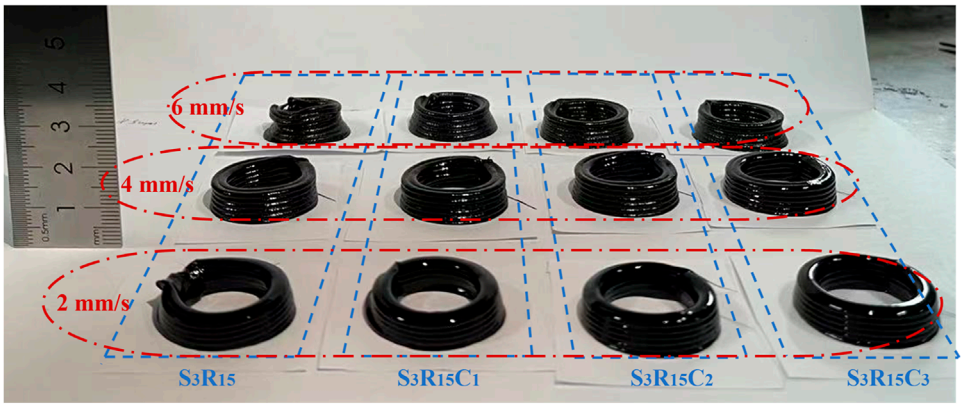

(B) Ring model printing results

FIGURE 11
Ring model and printing results of each modified asphalt binder under different temperatures. **(A)** Ring model for 3D printing. **(B)** Ring model printing results.

use circular modeling to explore the impact of printing speed on the shape of the composite-modified asphalt binder printability.

The bottom diameter of the simple circle model constructed using Simplify3D software is set to 2 cm, and the height is set to 1 cm. The model and the printing results are shown in Figures 11A, B. Figure 11B shows that the asphalt binder ring printed at a printing speed of 6 mm/s has a middle and high level of the outer wall concaved inward. To summarize the phenomenon of printing, there is, in the middle and high level of the outer wall of the asphalt binder ring, an inward depression, which is precisely because the printing speed is too fast, resulting in the new printing of asphalt binder material that has not been completely docked and adhered to the bottom of the layer. The asphalt binder material is removed from the nozzle, pulling the asphalt filament to the center of the circle to the inner movement of the outer wall of the situation caused by the invagination. When the printing speed was 4 mm/s, the shape of the printed asphalt binder circle was consistent with the model setup. When the printing speed was 2 mm/s, the asphalt binder ring tended to couch, the height became less than 1 cm, and the lines become rounded. A slight fusion of the upper and lower layers of the situation occurs, which is because the nozzle moves too slowly. However, at high temperature, the nozzle slightly softened the bottom of the asphalt binder, resulting in the slight collapse of the bottom, so that the printed asphalt binder specimens failed to reach the established height.

5 Conclusion

In this study, the impact of C9PR of 0 wt%, 1 wt%, 2 wt%, and 3 wt% on the rheological properties and 3D printability of modified asphalt binders was investigated. The key findings are as follows:

(1) FTIR and FM test results indicated that the reaction between C9PR, SBS, CR, and BA is mainly a physical reaction. C9PR can promote the swelling of SBS and CR particles in the asphalt binder, promoting compatibility by dispersing the modifier into smaller particles through high-speed shearing.

(2) $S_3R_{15}C_1$ exhibited the best high-temperature rutting resistance, elastic performance, and low-temperature ductility, but an excessive amount of C9PR weakened the performance of the modified asphalt binder.

(3) MSCR and LAS test results showed that $S_3R_{15}C_1$ maintained excellent high-temperature rutting resistance and fatigue

resistance after short-term and long-term aging. An appropriate amount of C9PR content promoted a more stable structure and improved the durability of the polymer-modified asphalt binder.

(4) The addition of C9PR facilitates smoother extrusion and molding of the SBS/CR composite-modified asphalt binder, reduces the lower limit of 3D-printable temperature, and enhances the construction and ease of use. For composite-modified asphalt binders prepared in this paper, the recommended printing temperature is 90°C, and the recommended printing speed is 4 mm/s.

In conclusion, this study investigated the effects of different contents of C9PR on the properties of the modified asphalt binder and revealed the potential application of C9PR as an additive for the 3D-printed asphalt binder. However, the optimal content of each polymer modifier and C9PR still needs to be explored. The use of modified asphalt binders for crack filling by 3D printing still needs to be practiced in engineering.

Data availability statement

The original contributions presented in the study are included in the article/Supplementary Material; further inquiries can be directed to the corresponding author.

Author contributions

YN: Methodology, Supervision, Writing–original draft, Writing–review and editing. XW: Data curation, Methodology, Writing–original draft. IB: Investigation, Writing–review and editing. DN: Methodology, Supervision, Writing–review and editing.

Funding

The author(s) declare that financial support was received for the research, authorship, and/or publication of this article. This study was financially supported by the National Natural Science Foundation of China (52278427), the Special Fund for Basic Scientific Research of Central Colleges, Chang'an University (300102310301), and the Natural Science Basic Research Program of Shaanxi (2024JC-YBMS-374).

Conflict of interest

The authors declare that the research was conducted in the absence of any commercial or financial relationships that could be construed as a potential conflict of interest.

Publisher's note

All claims expressed in this article are solely those of the authors and do not necessarily represent those of their affiliated organizations, or those of the publisher, the editors, and the reviewers. Any product that may be evaluated in this article, or claim that may be made by its manufacturer, is not guaranteed or endorsed by the publisher.

Supplementary material

The Supplementary Material for this article can be found online at: https://www.frontiersin.org/articles/10.3389/fmats.2024.1416246/full#supplementary-material

References

Aamer, N., Minchih, L., Yangwei, Z., and Nazir, U. (2022). Design and evaluation of asphalt concrete incorporating plastic aggregates fabricated using 3D printing technology. *3D Print. Addit. Manuf.* 9 (3), 212–222. doi:10.1089/3dp.2020.0347

Cai, C., Huang, W., and Lv, Q. (2014). Properties and application of terminal blending rubber asphalt. *J. Chongqing Jiaot. Univ. Sci.* 33 (4), 51–55. doi:10.3969/j.issn.1674-0696.2014.04.11

Cao, L., Yang, C., Dong, Z., Wang, W., and Yin, H. (2022). Aging mechanism of hot-poured sealants for asphalt pavement under natural environmental exposure. *Int. J. Pavement Eng.* 23 (2), 197–206. doi:10.1080/10298436.2020.1736296

Cong, Y., Xu, J., Huang, W., Zhang, C., and Liu, J. (2016). Study on modification of asphalt by SBS-C9 petroleum resin. *J. Build. Mater.* 19 (03), 602–605. doi:10.3969/j.issn.1007-9629.2016.03.032

Galooyak, S. S., Dabir, B., Nazarbeygi, A. E., and Moeini, A. (2010). Rheological properties and storage stability of bitumen/SBS/montmorillonite composites. *Constr. Build. Mater.* 24 (3), 300–307. doi:10.1016/j.conbuildmat.2009.08.032

Glover, C. J., Davison, R. R., Bullin, J. A., Estakhri, C. K., Williamson, S. A., Billiter, T. C., et al. (2000). *A comprehensive laboratory and field study of high-cure crumb-rubber modified asphalt materials*.

Gong, F., Cheng, X., Chen, Y., Liu, Y., and You, Z. (2022). 3D printed rubber modified asphalt as sustainable material in pavement maintenance. *Constr. Build. Mater.* 354, 129160. doi:10.1016/j.conbuildmat.2022.129160

Gong, F., Cheng, X., Fang, B., Cheng, C., Liu, Y., and You, Z. (2023). Prospect of 3D printing technologies in maintenance of asphalt pavement cracks and potholes. *J. Clean. Prod.* 397, 136551. doi:10.1016/j.jclepro.2023.136551

Gong, F., Cheng, X., Wang, Q., Chen, Y., You, Z., and Liu, Y. (2023). A review on the application of 3D printing technology in pavement maintenance. *Sustainability* 15 (7), 6237. doi:10.3390/su15076237

Hallmark-Haack, B. L., Hernández, N. B., Williams, R. C., and Cochran, E. W. (2019). Ground tire rubber modification for improved asphalt storage stability. *Energy and Fuels* 33, 2659–2664. doi:10.1021/ACS.ENERGYFUELS.8B03558

Hosseinnezhad, S., Kabir, S. F., Oldham, D., Mousavi, M., and Fini, E. H. (2019). Surface functionalization of rubber particles to reduce phase separation in rubberized asphalt for sustainable construction. *J. Clean. Prod.* 225, 82–89. doi:10.1016/j.jclepro.2019.03.219

Hou, X., Lv, S., Chen, Z., and Xiao, F. (2018). Applications of Fourier transform infrared spectroscopy technologies on asphalt materials. *Measurement* 121, 304–316. doi:10.1016/j.measurement.2018.03.001

Jackson, R. J., Wojcik, A., and Miodownik, M. (2018). 3D printing of asphalt and its effect on mechanical properties. *Mater. and Des.* 160, 468–474. doi:10.1016/j.matdes.2018.09.030

Kabir, S. F., Mousavi, M., and Fini, E. H. (2020). Selective adsorption of bio-oils' molecules onto rubber surface and its effects on stability of rubberized asphalt. *J. Clean. Prod.* 252, 119856. doi:10.1016/j.jclepro.2019.119856

Kim, H. H., Mazumder, M., Lee, M.-S., and Lee, S.-J. (2020). Laboratory evaluation of SBS modified asphalt binder containing GTR, SIS, and PE. *Adv. Civ. Eng.* 2020, 8830622. doi:10.1155/2020/8830622

Leng, Z., Padhan, R. K., and Sreeram, A. (2018). Production of a sustainable paving material through chemical recycling of waste PET into crumb rubber modified asphalt. *J. Clean. Prod.* 180, 682–688. doi:10.1016/j.jclepro.2018.01.171

Li, Z., Nie, X., Yao, H., Zhou, H., and Li, C. (2019). Study on properties of C9 petroleum resin/SBS composite modified asphalt. *J. Build. Mater.* 22 (05), 764–770. doi:10.3969/j.issn.1007-9629.2019.05.014

Li, F., Zhou, S., Cai, W., Du, Y., and Li, L. (2017). Laboratory evaluation of short and long term performance of hot-poured sealants. *Constr. Build. Mater.* 148, 30–37. doi:10.1016/j.conbuildmat.2017.05.014

Li J., J., Xiao, F., and Amirkhanian, S. N. (2019). Storage, fatigue and low temperature characteristics of plasma treated rubberized binders. *Constr. Build. Mater.* 209, 454–462. doi:10.1016/j.conbuildmat.2019.03.136

Ma, G., Wang, L., and Ju, Y. (2017). State-of-the-art of 3D printing technology of cementitious material—an emerging technique for construction. *Sci. China Technol. Sci.* 61, 475–495. doi:10.1007/s11431-016-9077-7

Mturi, G. A. J., O'Connell, J., Zoorob, S. E., and De Beer, M. (2014). A study of crumb rubber modified bitumen used in South Africa. *Road Mater. Pavement Des.* 15 (4), 774–790. doi:10.1080/14680629.2014.910130

Nie, X., Hou, T., Yao, H., Li, Z., Zhou, X., and Li, C. (2019a). Effect of C 9 petroleum resins on improvement in compatibility and properties of SBS-modified asphalt. *Petroleum Sci. Technol.* 37, 1704–1712. doi:10.1080/10916466.2019.1602642

Nie, X., Yao, H., Li, C., Zhou, H., and Li, C. (2019b). Effect of C9 petroleum resins on the performance of high-viscosity asphalt. *Acta Pet. Sin. Process. Sect.* 35 (01), 176–182. doi:10.1080/10916466.2019.1602642

Park, S. W., Richard Kim, Y., and Schapery, R. A. (1996). A viscoelastic continuum damage model and its application to uniaxial behavior of asphalt concrete. *Mech. Mater.* 24 (4), 241–255. doi:10.1016/S0167-6636(96)00042-7

Presti, D. L. (2013). Recycled Tyre Rubber Modified Bitumens for road asphalt mixtures: a literature review. *Constr. Build. Mater.* 49, 863–881. doi:10.1016/j.conbuildmat.2013.09.007

Presti, D. L., Airey, G., and Partal, P. (2012). Manufacturing terminal and field bitumen-tyre rubber blends: the importance of processing conditions. *Procedia - Soc. Behav. Sci.* 53, 485–494. doi:10.1016/j.sbspro.2012.09.899

Qian, C., Fan, W., Liang, M., Nan, G., and Luo, H. (2018). Influence of compatibilizer composition on performance of SBS modified asphalt. *AIP Conf. Proc.* 1971 (1). doi:10.1063/1.5041202

Qian, C., Fan, W., Ren, F., Lv, X., and Xing, B. (2019). Influence of polyphosphoric acid (PPA) on properties of crumb rubber (CR) modified asphalt. *Constr. Build. Mater.* 227, 117094. doi:10.1016/j.conbuildmat.2019.117094

Rowe, G. M., and Sharrock, G. (2009). *Functional forms for master curve analysis of bituminous materials*.

Shatnawi, S. R., and President, E. (2010). *Comparisons of rubberized asphalt binders asphalt-rubber and terminal blend for the rubber*.

Wu, H., Chen, P., Chen, C., and Zhang, W. (2022). Effect of aromatic petroleum resin on microstructure of SBS modified asphalt. *Adv. Mater. Sci. Eng.* 2022, 1–11. doi:10.1155/2022/5136748

Wu, X. (2023). Preparation and performance study of modified polyurethane sealant based on 3D printing. doi:10.26976/d.cnki.gchau.2023.000208

Xu, O., Rangaraju, P. R., Wang, S., and Xiao, F. (2017). Comparison of rheological properties and hot storage characteristics of asphalt binders modified with devulcanized ground tire rubber and other modifiers. *Constr. Build. Mater.* 154, 841–848. doi:10.1016/j.conbuildmat.2017.07.221

Xue, Y. (2023). *Preparation and properties of SBS/LNBR/CR modified asphalt for 3D crack repairing*. doi:10.26976/d.cnki.gchau.2023.001645

Yang, H. (2023). *Preparation and performance of 3D printable TPSiV/SBS/CR composite modified asphalt sealant*. doi:10.26976/d.cnki.gchau.2023.001549

Yu, J., Ren, Z., Yu, H., Wang, D., Svetlana, S., Korolev, E., et al. (2018). Modification of asphalt rubber with nanoclay towards enhanced storage stability. *Materials* 11 (11), 2093. doi:10.3390/ma11112093

Yusoff, N. I. M., Chailleux, E., and Airey, G. (2011). A comparative study of the influence of shift factor equations on master curve construction. *Int. J. pavement Res. Technol.* 4, 324–336. doi:10.6135/IJPRT.ORG.TW/2011.4(6).324

Zhang, J., Huang, W., Zhang, Y., Yan, C., Lv, Q., and Guan, W. (2021). Evaluation of the terminal blend crumb rubber/SBS composite modified asphalt. *Constr. Build. Mater.* 278, 122377. doi:10.1016/j.conbuildmat.2021.122377

Zhang, L., Hoff, I., Zhang, X., Liu, J., Yang, C., and Wang, F. (2023). A methodological review on development of crack healing technologies of asphalt pavement. *Sustainability* 15 (12), 9659. doi:10.3390/su15129659

Zhang, W., Qiu, L., Liu, J., Hu, K., Zou, L., Chen, Y., et al. (2021). Modification mechanism of C9 petroleum resin and its influence on SBS modified asphalt. *Constr. Build. Mater.* 306, 124740. doi:10.1016/j.conbuildmat.2021.124740

Zhao, M., and Dong, R. (2021). Reaction mechanism and rheological properties of waste cooking oil pre-desulfurized crumb tire rubber/SBS composite modified asphalt. *Constr. Build. Mater.* 274, 122083. doi:10.1016/j.conbuildmat.2020.122083